



Syntheses and characterization of four 2D metal–organic networks based on rigid imidazolate/carboxylate functionalized ligand – Effect of the torsion of the ligands on crystal structures and properties

Jing-Si Yang^a, Jiang Zhu^b, Rui-Bin Liu^a, Jun Ni^a, Zhi-Duo Chang^a, Tao Hu^a, Jian-Jun Zhang^{a,*}, Chang-Gong Meng^a

^a Chemistry College, Dalian University of Technology, Dalian 116024, China

^b School of Chemistry and Chemical Engineering, Liaoning Normal University, Dalian 116029, China

ARTICLE INFO

Article history:

Received 25 March 2012
Received in revised form 10 July 2012
Accepted 25 July 2012
Available online 11 August 2012

Keywords:

Supramolecular
Self-assembly
Carboxylate
Coordination polymer
Thermal stability

ABSTRACT

A series of rigid imidazolate/carboxylate functionalized ligands, X-(5,7-dioxopyrrolo[3,4-f]benzimidazole-6-yl)benzoic acid (X = 4, H₂4-DPBB; X = 3, H₂3-DPBB; X = 2, H₂2-DPBB) were designed and used for the assemble reactions with Zn²⁺/Cd²⁺/Cu²⁺ ions. Four compounds, [Zn(4-DPBB)(H₂O)]·DMSO·0.5MeOH (**1**), [Cd(3-DPBB)(DMA)_{1.8}(H₂O)_{0.2}] (**2**), [Cu(3-DPBB)(DMSO)(DMA)] (**3**) and [Cd(2-DPBB)(DMA)₂] (**4**) have been synthesized and structurally characterized (where DMSO = dimethylsulfoxide, DMA = dimethyl acetamide). Single crystal X-ray analyses show that the four compounds are all based on 3-connected single metal nodes and 3-connected spacers. Compounds **1** and **2** bear a 2D (6, 3)-net structure, while **3** and **4** have a 2D (4, 8)-net. Compared with **2**, **3** and **4**, **1** exhibits a relatively high thermal stability which is up to ~550 °C. Luminescent analysis indicates that **1** and **2** exhibit linker-localized emissions while **4** has ligand-to-metal charge transfer (LMCT) emission. The effect of the torsion of the ligands on the crystal structures and properties of the four compounds is discussed.

© 2012 Elsevier B.V. All rights reserved.

1. Introduction

In the past two decades great progress has been made in the development of metal organic materials (MOMs) that incorporate inorganic and organic components within a single material through supramolecular interaction such as coordination bond, hydrogen bond and π - π stacking interaction [1–7]. Most compounds have been prepared for developing new porous materials and structures with potential applications traditionally observed in inorganic zeolites, such as size- and shape-selective uptake, catalysis, separation, and gas storage [1–7]. However, better comprehension of the correlation between syntheses, structure and application remains a great challenge due to some uncertain effect factors, including experimental conditions, geometries of molecular building blocks (MBBs), bridging modes of the ligands etc. [8–10].

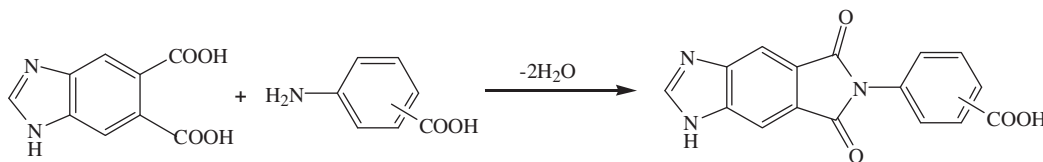
Most synthesized MOMs are based on polycarboxylates, polypyridinates/imidazolates, pyrazolate derivatives and phosphonates ligands [11–16]. The coordination chemistry of aromatic polycarboxylate ligands has been well explored owing to their relatively strong coordination ability and a variety of bridging modes coordinating to almost all the metal ions, as well as the diverse structure

type and the potential of exploiting properties of the MOMs thus formed [6,7]. On the other hand, imidazole and its derivations are characterized by their special N, N-donor set. Coordinated by tetrahedral metal ions (e.g., Zn, Co), the ligands can be used to construct a special type of MOMs with zeolite-type tetrahedral topologies [17–22]. At the same time, MOMs based on imidazolate/carboxylate ligand were also well studied. A typical example is 4, 5-imidazoledicarboxylic acid which has been used for the construction of 3D anionic frameworks through a single-metal-ion based molecular building block (MBB) in the presence of different cationic structure direction agents [23,24]. However, in marked contrast to the extensive studies of imidazole and its short carboxylate-substituted derivations, few long rigid imidazolate/carboxylate ligands have been reported in MOMs synthesis [23–27].

Compared with other properties, thermal stability of MOMs is less concerned because only a few reported MOMs remain stable up to 450 °C, even though this property is very important for practical applications [28–31]. Herein we present the design and synthesis of a series of new long rigid ligands containing imidazolate/carboxylate groups (Scheme 1). The assemble reactions with different metal ions were well investigated and four new 2D frameworks possessing (6, 3) or (4, 8) net structure were obtained: [Zn(4-DPBB)(H₂O)]·DMSO·0.5MeOH (**1**), [Cd(3-DPBB)(DMA)_{1.8}(H₂O)_{0.2}] (**2**), [Cu(3-DPBB)(DMSO)(DMA)] (**3**) and [Cd(2-DPBB)(DMA)₂] (**4**). The series of ligands provide a good model to

* Corresponding author. Tel.: +86 411 84986036.

E-mail address: zhangjj@dlut.edu.cn (J.-J. Zhang).



Scheme 1. Syntheses of the ligands.

investigate the effect of the torsion of the ligands (the substituted site of the carboxylate group on benzene ring) on the crystal structures and properties of the MOMs based on the ligands. Details of crystal structures and properties are discussed.

2. Experimental

2.1. Materials and instrumentation

Starting materials were of reagent grade and used without further purification. X-ray powder diffraction patterns were collected on a D/MA α -2400 diffractometer using Cu K α radiation ($\lambda = 1.54056 \text{ \AA}$) under ambient conditions. FT-IR spectra were recorded in the range of 4000–400 cm^{-1} on a Centauri spectrometer with KBr pellets. Elemental analyses were determined using a Vario EL III elemental analyzer. Thermogravimetric analysis (TGA) was recorded with a NETZSCH STA 449F3 unit at a heating rate of 10 $^{\circ}\text{C}/\text{min}$ under nitrogen atmosphere. Electrospray ionization-mass spectroscopy (ESI-MS) analysis was carried out with HP 1100LC/MSD liquid chromatograph-mass spectrometer. ^1H nuclear magnetic resonance (NMR) were recorded on a Bruker Avancell400M spectrometer. Melting points analyses were carried out with micro melting point analysis X-6 in the range of 25–310 $^{\circ}\text{C}$.

2.2. Synthesis

2.2.1. $\text{H}_2\text{A-DPBB}$

A mixture of benzimidazole-5,6-dicarboxylic acid (2.0616 g, 10 mmol) and 4-aminobenzoic acid (1.3714 g, 10 mmol) in 30 ml DMF was heated at 135 $^{\circ}\text{C}$ for 10 h, then filtrated. The product was washed several time with hot DMF and EtOH, then dried in air. Yield: 70%. Element analysis (%): *Anal. Calc.* for $\text{C}_{16}\text{H}_9\text{N}_3\text{O}_4$: C 62.54, H 2.95, N 13.68. Found: C 62.55, H 2.91, N 13.65%. IR (KBr pellet, cm^{-1}): 3340(m), 3050(s), 1770(m), 1713(vs), 1605(m), 1509(m), 1371(vs), 1264(vs), 1118(m), 865(s), 835(s), 610(s). Negative ESI-MS (m/z): 305.98 ($\text{H}_2\text{A-DPBB-H}^+$). ^1H NMR (DMSO- d_6): δ : 7.630 ($J = 4.8 \text{ Hz}$, d, 2H, Ph-H), 8.097 ($J = 1.2 \text{ Hz}$, d, 2H, Ph-H), 8.114 (s, 1H, Ph-H), 8.208 (s, 1H, Ph-H), 8.602 (s, 1H, Im-H), 13.320 (s, 1H, COOH). Melting points: above 300 $^{\circ}\text{C}$.

2.2.2. $\text{H}_2\text{B-DPBB}$

The above mentioned synthesis procedure was repeated except 3-aminobenzoic acid was used. Yield: 65.5%. Element analysis (%): *Anal. Calc.* for $\text{C}_{16}\text{H}_9\text{N}_3\text{O}_4$: C 62.54, H 2.95, N 13.68. Found: C 62.60, H 2.92, N 13.69%. IR (KBr pellet, cm^{-1}): 3310(m), 2520(m), 1780(vs), 1670(vs), 1600(m), 1550(m), 1480(vs), 1090(vs), 840(m), 776(m), 673(s), 543(s). Negative ESI-MS (m/z): 305.88 ($\text{H}_2\text{B-DPBB-H}^+$). ^1H NMR (DMSO- d_6): δ : 7.669 ($J = 1.6 \text{ Hz}$, t, 1H, Ph-H), 7.747 ($J = 7.2 \text{ Hz}$, d, 1H, Ph-H), 7.995 ($J = 8.0 \text{ Hz}$, d, 1H, Ph-H) 8.057 (s, 1H, Ph-H) 8.104 (s, 1H, Ph-H) 8.201 (s, 1H, Ph-H), 8.596 (s, 1H, Im-H), 13.293 (s, 1H, COOH). Melting points: above 300 $^{\circ}\text{C}$.

2.2.3. $\text{H}_2\text{C-DPBB}$

The above mentioned synthesis procedure was repeated except 2-aminobenzoic acid was used. White solid was obtained upon

adding equal amount of water to the filtrate solution. The product was filtrated, washed several time with hot DMF and EtOH, then dried in air. Yield: 56%. Element analysis (%): *Anal. Calc.* for $\text{C}_{16}\text{H}_9\text{N}_3\text{O}_4$: C 62.54, H 2.95, N 13.68. Found: C 62.59, H 2.93, N 13.70%. IR (KBr pellet, cm^{-1}): 3340(m), 3050(s), 1768(m), 1710(vs), 1600(m), 1511(m), 1383(vs), 1112(m), 835(w), 767(m), 745(s), 695(s). Negative ESI-MS (m/z): 305.85 ($\text{H}_2\text{C-DPBB-H}^+$). ^1H NMR (DMSO- d_6): δ : 7.527 ($J = 8.0, 1.2 \text{ Hz}$, dd, 1H, Ph-H), 7.622 ($J = 16.0, 1.2 \text{ Hz}$, td, 1H, Ph-H), 7.773 ($J = 16.0, 1.2 \text{ Hz}$, td, 1H, Ph-H), 8.045 ($J = 8.0, 1.2 \text{ Hz}$, dd, 1H, Ph-H), 8.105 (s, 1H, Ph-H), 8.183 (s, 1H, Ph-H), 8.598 (s, 1H, Im-H), 13.305 (s, 1H, COOH). Melting points: 295.4–296.7 $^{\circ}\text{C}$.

2.2.3.1. $[\text{Zn}(4\text{-DPBB})(\text{H}_2\text{O})]\cdot\text{DMSO}\cdot 0.5\text{MeOH}$ (**1**). Equimolar amounts of $\text{H}_2\text{A-DPBB}$ (0.0061 g, 0.02 mmol) and $\text{Zn}(\text{NO}_3)_2\cdot 6\text{H}_2\text{O}$ (0.0059 g, 0.02 mmol) in a solvent mixture of DMSO/DMF/MeOH (1 ml/0.5 ml/0.5 ml) were placed in a 20 ml scintillation vial, heated to 85 $^{\circ}\text{C}$ for 24 h, then cooled to room temperature. The colorless crystals were collected, washed with DMSO and dried in air (53% yield). Element analysis (%): *Anal. Calc.* for $\text{C}_{18.5}\text{H}_{17}\text{N}_3\text{O}_{6.5}\text{SZn}$: C 46.02, H 3.55, N 8.70. Found: C 45.95, H 3.82, N 8.59%. IR (KBr pellet, cm^{-1}): 3440(m), 3114(w), 1772(s), 1708(vs), 1608(vs), 1538(m), 1409(m), 1357(vs), 1187(vs), 1022(s), 846(s), 784(m), 744(s), 613(w), 460(m).

2.2.3.2. $[\text{Cd}(3\text{-DPBB})(\text{DMA})_{1.8}(\text{H}_2\text{O})_{0.2}]$ (**2**). $\text{H}_2\text{B-DPBB}$ (0.0246 g, 0.08 mmol) and $\text{Cd}(\text{NO}_3)_2\cdot 4\text{H}_2\text{O}$ (0.0247 g, 0.08 mmol) in a solvent mixture of DMA/ H_2O (3 ml/0.5 ml) were placed in a 20 ml scintillation vial, heated to 125 $^{\circ}\text{C}$ for 12 h, then cooled to room temperature. The colorless crystals were collected, washed with DMA and dried in air (49% yield). Element analysis (%): *Anal. Calc.* for $\text{C}_{23.2}\text{-H}_{23.6}\text{CdN}_{4.8}\text{O}_6$: C 48.20, H 4.11, N 11.63. Found: C 48.25, H 4.26, N 11.87%. IR (KBr pellet, cm^{-1}): 3454(w), 1766(m), 1706(vs), 1603(vs), 1547(m), 1455(m), 1400(vs), 1308(m), 1308(m), 1021(m), 853(m), 758(m), 745(m), 650(m), 630(m), 616(m).

2.2.3.3. $[\text{Cu}(3\text{-DPBB})(\text{DMSO})(\text{DMA})]$ (**3**). Equimolar amounts of $\text{H}_2\text{B-DPBB}$ (0.0246 g, 0.08 mmol) and $\text{Cu}(\text{NO}_3)_2\cdot 3\text{H}_2\text{O}$ (0.0193 g, 0.08 mmol) in a solvent mixture of DMSO/DMA/ H_2O (2 ml/1 ml/0.5 ml) were placed in a 20 ml scintillation vial, heated to 85 $^{\circ}\text{C}$ for 24 h, then cooled to room temperature. The green crystals were collected, washed with DMA and dried in air (57% yield). Element analysis (%): *Anal. Calc.* for $\text{C}_{22}\text{H}_{22}\text{N}_4\text{O}_6\text{SCu}$: C 49.48, H 4.15, N 10.49. Found: C 49.25, H 4.15, N 10.47%. IR (KBr pellet, cm^{-1}): 1760(m), 1700(vs), 1610(vs), 1480(m), 1360(s), 1310(m), 1190(m), 1110(m), 996(s), 959(m), 851(m), 760(m), 671(m), 627(m), 453(m).

2.2.3.4. $[\text{Cd}(2\text{-DPBB})(\text{DMA})_2]$ (**4**). Equimolar amounts of $\text{H}_2\text{C-DPBB}$ (0.0061 g, 0.02 mmol) and $\text{Cd}(\text{OAc})_2\cdot 2\text{H}_2\text{O}$ (0.0213 g, 0.08 mmol) in a solvent mixture of DMA/EtOH (3 ml/0.1 ml) were placed in a 20 ml scintillation vial, heated to 105 $^{\circ}\text{C}$ for 24 h, then cooled to room temperature. The colorless crystals were collected, washed with DMA and dried in air (39% yield). Element analysis (%): *Anal. Calc.* for $\text{C}_{24}\text{H}_{25}\text{N}_5\text{O}_6\text{Cd}$: C 48.70, H 4.26, N 11.83. Found: C 48.24, H

4.27, N 11.91%. IR (KBr pellet, cm^{-1}): 1774(m), 1712(vs), 1656(m), 1588(m), 1541(m), 1487(w), 1397(vs), 1373(vs), 1306(m), 1193(w), 1121(s), 955(m), 884(m), 847(m), 782(m), 758(m), 744(m), 710(m), 666(m), 628(m), 420(m).

2.2.3.5. X-ray structure determinations. Intensity data were measured at 293(2) K on a Bruker SMART APEX II CCD area detector system. Data reduction and unit cell refinement were performed with Smart-CCD software [32]. The structures were solved by direct methods using SHELXS-97 and were refined by full-matrix least squares methods using SHELXL-97 [33].

For **1**, all nonhydrogen atoms were refined anisotropically. No attempts were made to locate the hydrogen atoms on the half occupied MeOH molecules. The hydrogen atoms related to carbon atoms were generated geometrically. The maximum residual peak and hole on the final difference electron density map were found to be $1.276 \text{ e}^{-}/\text{\AA}^3$ (0.30 Å from S1) and $-1.000 \text{ e}^{-}/\text{\AA}^3$ (1.14 Å from S1), respectively. For **2**, all nonhydrogen atoms were refined anisotropically. The hydrogen atoms related to carbon atoms were generated geometrically. The coordinated water molecule and one of the coordinated DMA molecules share the same oxygen atom. Partial occupancy refinement was performed and the best refinement result is 0.8DMA and 0.2H₂O. The maximum residual peak and hole on the final difference electron density map were found to be $0.942 \text{ e}^{-}/\text{\AA}^3$ (0.84 Å from N4) and $-0.407 \text{ e}^{-}/\text{\AA}^3$ (0.27 Å from N4), respectively. For **3**, all nonhydrogen atoms were refined anisotropically. The hydrogen atoms related to carbon atoms were generated geometrically. The maximum residual peak and hole on the final difference electron density map were found to be $0.513 \text{ e}^{-}/\text{\AA}^3$ (1.05 Å from C19) and $-0.512 \text{ e}^{-}/\text{\AA}^3$ (0.47 Å from C18), respectively. For **4**, all non hydrogen atoms were refined anisotropically. The hydrogen atoms related to carbon atoms were generated geometrically. The maximum residual peak and hole on the final difference electron density map were found to be $0.404 \text{ e}^{-}/\text{\AA}^3$ (1.09 Å from Cd1) and $-0.281 \text{ e}^{-}/\text{\AA}^3$ (0.65 Å from H17B), respectively.

A summary of the most important crystal and structure refinement data is given in Table 1.

3. Results and discussion

3.1. Crystal structure of **1**

The structure of **1** is a 2D coordination polymer that based on 3-connected Zn²⁺ nodes and 4-DPBB ligands (Fig. 1). Each Zn²⁺ ion is four-coordinated with 2 N atoms from 2 ligands, 1 O atom from carboxylate group of one ligand and 1 O atom from one coordinated water molecule. The Zn–O_{H₂O} bond distance is 1.973(6) Å, a little longer than that for Zn–O_{COOH} (1.960(6) Å). The Zn–N_{im} bond distances are in the range of 1.976(6)–1.991(6) Å. To Zn(1), small deviations of bond angles from the idealized tetrahedral geometry are found for angles O(1A)–Zn(1)–O(5) [107.6(3)°], O(1A)–Zn(1)–N(1) [124.2(2)°], O(5)–Zn(1)–N(1) [108.2(2)°], O(5)–Zn(1)–N(2B) [106.6(3)°] and N(1)–Zn(1)–N(2B) [112.4(3)°], implying the metal ion in a distorted tetrahedral coordination polyhedron.

Two imidazole nitrogen atoms in each ligand coordinate to two metal ions and one carboxylate oxygen atom coordinates to the third Zn²⁺ ion. A 46.6° dihedral angle is observed between the benzimidazole and benzene rings for the ligand.

The combination of the 3-connected Zn(II) nodes and the ligands lead to the neutral 2D layer with a thickness of 6.39 Å and the structure may be described as a (6, 3) honeycomb-type net. The layers are packed along the *ac* plane and separated by free DMSO and disordered water solvent molecules. Inside the layer, the Zn...Zn distances are 5.82 (bridged by the imidazole group), 15.04 and 15.13 Å, respectively. Due to the torsion of the ligand, the 2D net bears a wave-like structure motif with a corresponding angle of 56.07°. The surface of the net are decorated with oxygen atoms, either from the coordinated water molecules or uncoordinated carboxylate or carbonyl groups, which makes the net hydrophilic. Hydrogen bonds between the coordinated water molecules and oxygen atoms link the 2D nets into a 3D frameworks (O5...O2 = 2.63(1) Å, ∠O5–H5B...O2 = 173(9)°, symmetry code for O2: $-x+2, -y, -z+2$). Hydrogen bonds also help to stabilize the free DMSO molecules (O5...O6 = 2.63(1) Å, ∠O5–H5A...O6 = 139(8)°, symmetry code for O6: $-x+2, -y, -z+2$).

Table 1
Crystal data and structure refinement for the complexes.

	1	2	3	4
Formula	C _{18.5} H ₁₇ ZnN ₃ O _{6.5} S	C _{23.2} H _{23.6} CdN _{4.8} O ₆	C ₂₂ H ₂₂ CuN ₄ O ₆ S	C ₂₄ H ₂₅ CdN ₅ O ₆
Formula weight	482.78	578.07	534.04	591.89
Crystal system	monoclinic	monoclinic	monoclinic	monoclinic
Space group	P2(1)/c	P2(1)/n	P2(1)/n	P2(1)/c
<i>a</i> (Å)	15.13(3)	14.601(2)	11.7035(6)	15.286(2)
<i>b</i> (Å)	13.94(2)	7.721(1)	8.6041(5)	9.216(1)
<i>c</i> (Å)	10.34(2)	22.842(3)	23.7693(11)	18.137(2)
α (°)	90	90	90	90
β (°)	103.61(2)	95.446(2)	91.709(4)	104.793(1)
γ (°)	90	90	90	90
<i>V</i> (Å ³)	2121(6)	2563.6(6)	2392.5(2)	2470.3(5)
<i>Z</i>	4	4	4	4
<i>D</i> _{calc} (g/cm ³)	1.512	1.498	1.483	1.591
<i>F</i> (000)	988	1170	1100	1200
θ (°)	2.01–25.00	2.79–25.00	1.71–25.00	2.32–25.50
Reflections collected	9934	12285	15630	11820
Unique	3711	4494	3965	4576
<i>R</i> _{int}	0.1279	0.0330	0.0454	0.0270
Goodness-of-fit (GOF) on <i>F</i> ²	0.993	0.980	1.086	1.045
<i>R</i> ₁ ^a , <i>wR</i> ₂ [*]				
<i>I</i> > 2σ (<i>I</i>)	<i>R</i> ₁ = 0.0807, <i>wR</i> ₂ = 0.1699	<i>R</i> ₁ = 0.0391, <i>wR</i> ₂ = 0.1037	<i>R</i> ₁ = 0.0434, <i>wR</i> ₂ = 0.0987	<i>R</i> ₁ = 0.0282, <i>wR</i> ₂ = 0.0687
All data	<i>R</i> ₁ = 0.1744, <i>wR</i> ₂ = 0.1966	<i>R</i> ₁ = 0.0524, <i>wR</i> ₂ = 0.1124	<i>R</i> ₁ = 0.0659, <i>wR</i> ₂ = 0.1061	<i>R</i> ₁ = 0.0377, <i>wR</i> ₂ = 0.0727
Maximum/mean shift in final cycle	0.000/0.000	0.000/0.000	0.001/0.000	0.001/0.000

^a *R*₁ = (|*F*_o − |*F*_c||)/|*F*_o||, ^{*}*wR*₂ = {*w* [(*F*_o² − *F*_c²)]/*w* [(*F*_o²)]^{0.5}, *w* = [σ(*F*_o²) + (*aP*)² + *bP*]^{−1}, where *P* = (*F*_o² + 2 *F*_c²)/3]. 1: *a* = 0.0375, *b* = 0.1804; 2: *a* = 0.0690, *b* = 1.1851; 3: *a* = 0.0516, *b* = 0.5409; 4: *a* = 0.0789, *b* = 0.0000.

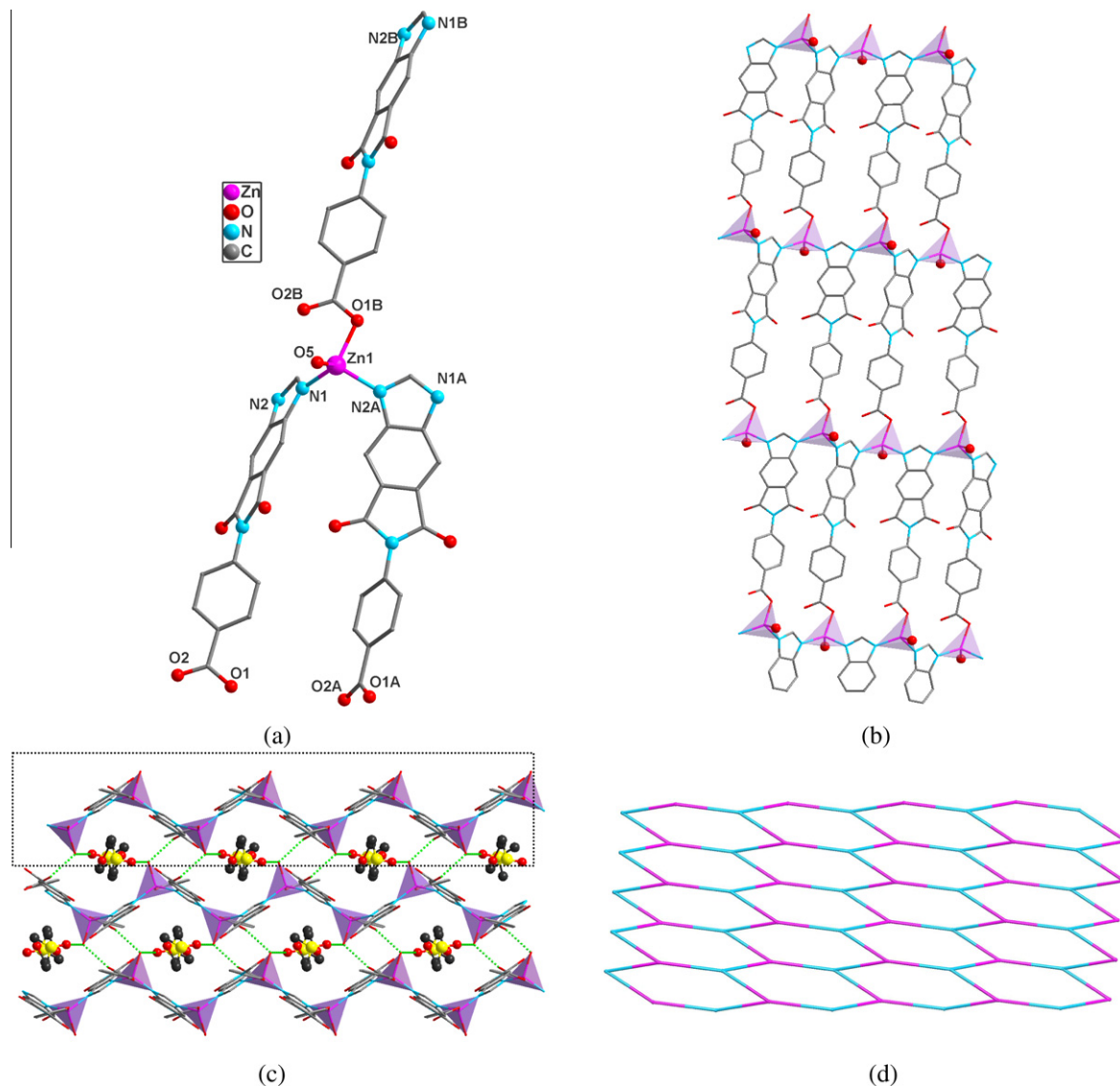


Fig. 1. The structure of compound **1**. (a) The coordination environment of the Zn^{2+} ion. Symmetry code: A: $-x + 3/2, y - 1/2, -z + 3/2$; B: $x + 1, y, z$; (b) the 2D layer structure viewed along the b direction; (c) the packing diagram viewed along the a direction; the atoms of framework are shown in wires mode while those of free DMSO molecules are shown in ball and stick mode; (d) The framework topology of the 2D net.

3.2. Crystal structure of **2**

2 Features two-dimensional (6, 3) network with 3-connected Cd^{2+} and 3-DPBB ligands as nodes. Fig. 2a shows the coordination environment of Cd^{2+} ion. The 6-coordinated Cd^{2+} center is in a slightly distorted octahedral coordination environment that is coordinated by 2 N atoms from 2 ligands, 2 O atoms from carboxylate group of one ligand and 2 O atoms from 2 coordinated solvent molecules. The bond angles around Cd^{2+} ion range from $54.95(9)$ to $178.57(1)^\circ$. The Cd–O and Cd–N bond distances are in the range of $2.250(3)$ – $2.485(5)$ and $2.211(3)$ – $2.261(3)$ Å, respectively. All are consistent with the values reported for Cd–carboxylate and Cd–imidazole complexes [27,28]. Three Cd^{2+} ions are connected by a 3-DPBB ligand with $\mu_3\text{-}\eta^2$: η^1 : η^1 coordination mode (Scheme 1b), in which the carboxylate group chelate one Cd^{2+} ion in monobidentate mode and each ligand also uses two imidazole nitrogen atoms to coordinate to two other metal ions. A 46.14° dihedral angle is also observed between the benzimidazole and benzene rings.

Each ligand is bound to three Cd^{2+} ions and each Cd^{2+} ion is also linked by three ligands. These give rise to a neutral 2D (6, 3) net perpendicular to the c direction. When viewed along the a direction the 2D net is ruffled to create a zigzag structural motif and the coordinated DMA molecules are used to fill the breach of the net. Inside the layer, the Cd...Cd separations are 6.23 (bridged by the imidazole group), 12.59 and 14.60 Å, respectively. The 2D nets are packed along the c direction to form the overall structure and a schematic representation of the 2D honeycomb-type net is shown in Fig. 2d.

3.3. Crystal structure of **3**

3 Possesses 2D nets built of 3-connected Cu^{2+} nodes and 3-DPBB ligands (Fig. 3). Each Cu^{2+} ion has a $\{\text{N}_2\text{O}_3\}$ donor set and square plane is composed of 2 N atoms from 2 ligands, 1 O atom from the carboxylate group of the third ligand and another oxygen atom from a coordinated DMSO molecule. The Cu–O and Cu–N bond distances are in the range of $1.945(2)$ – $2.009(2)$ and

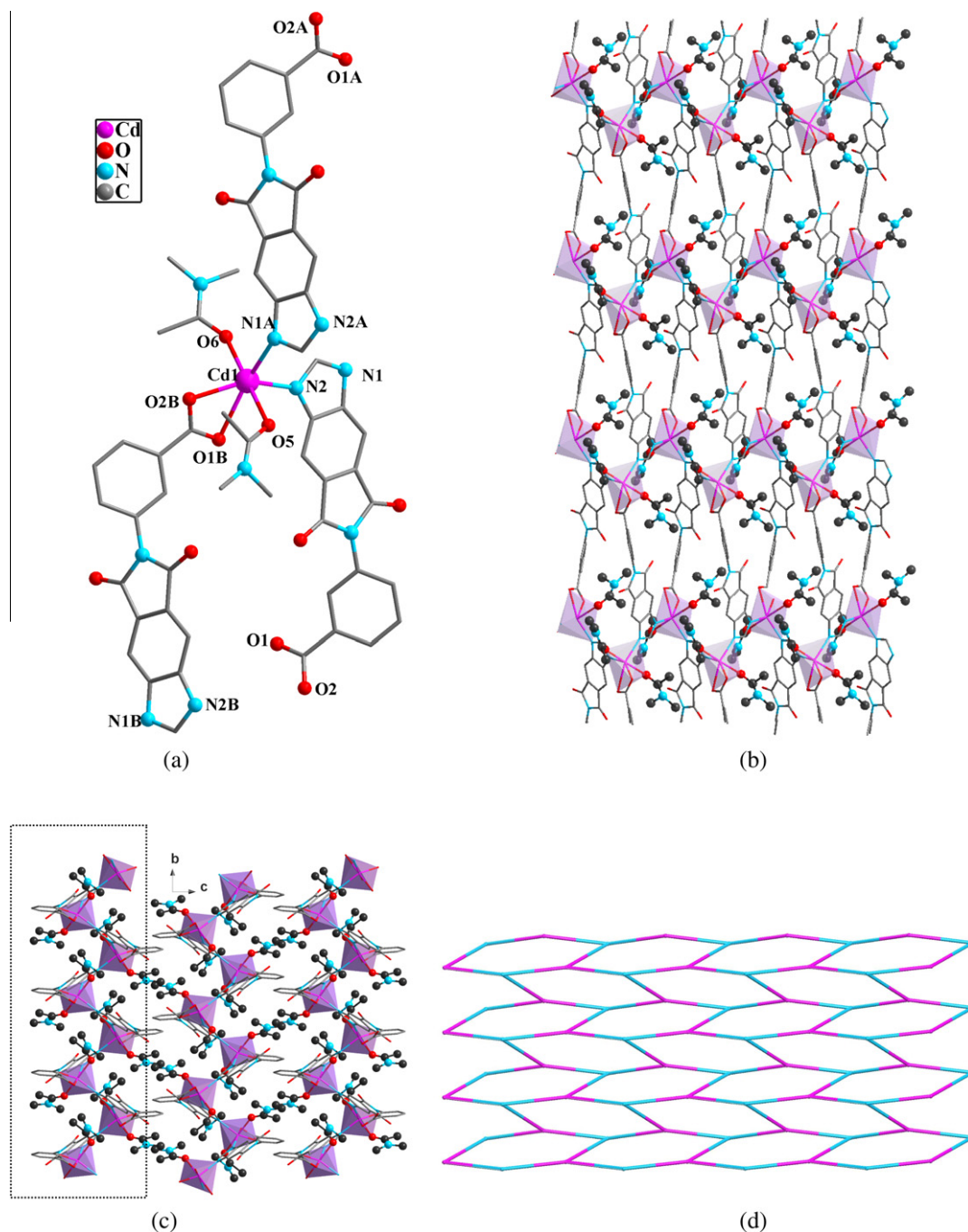


Fig. 2. The structure of compound **2**. (a) The coordination environment of the Cd²⁺ ion. Symmetry code: A: $-x + 3/2, y - 1/2, -z + 3/2$; B: $x + 1, y, z$; (b) the 2D layer structure viewed along the *b* direction. The atoms of framework are shown in wires mode while those of coordinated solvent molecules are shown in ball and stick mode; (c) the 2D layer structure viewed along the *a* direction; (d) the framework topology of the 2D net.

1.991(2)–2.002(3) Å, respectively. A slightly square-pyramidal configuration around the Cu²⁺ ion is completed by the additional binding of one DMA molecule in axial position (Cu–O6 = 2.486 Å). The Cu²⁺ ion deviates by about 0.03 Å from the least squares plane defined by N1, N2, O3 and O5 toward the coordinated DMA molecule. The bond angles around Cu²⁺ ion range from 86.2(1) to 177.95(9)°. Each ligand uses two imidazole nitrogen atoms to coordinate to two metal ions and one carboxylate oxygen atom to coordinate to the third Cu²⁺ ion. A 68.95° dihedral angle is observed between the benzimidazole and benzene rings.

Each ligand is bound to three Cu²⁺ ions and each Cu²⁺ ion is also linked by three ligands. Thus a neutral 2D (4, 8) distorted network is formed. Coordinated DMA and DMSO molecules are used to fill

the breach of the net (Fig. 3). Inside the layer, the Cu...Cu separations are 5.98 (bridged by the imidazole group), 12.49 and 13.45 Å, respectively. The packing of the 2D nets and a schematic representation of the net is shown in Fig. 3d.

3.4. Crystal structure of **4**

The structure of **4** may be described as a 2D net based on 3-connected Cd²⁺ nodes and 2-DPBB ligands (Fig. 4). Selected bond distances and angles are shown in Table 2. In the structure each Cd²⁺ ion is 6-coordinated with 2 imidazole N atoms from 2 ligands, 2 O atoms from carboxylate group of one ligand and 2 O atoms from 2 coordinated disordered DMA molecules respectively. The

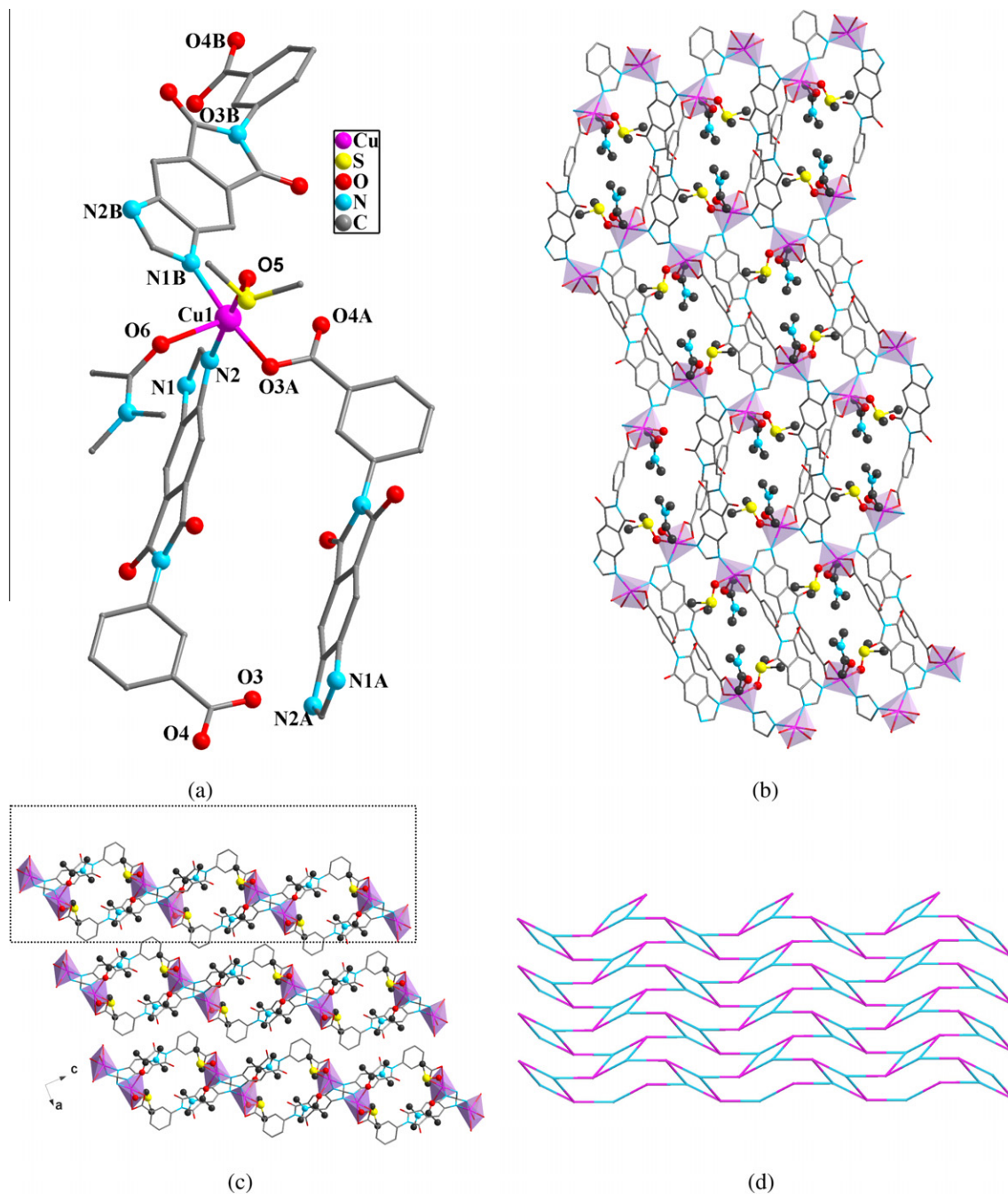


Fig. 3. The structure of compound **3**. (a) The coordination environment of the Cu²⁺ ion. Symmetry code: A: $x - 1/2, -y + 3/2, z - 1/2$; B: $-x + 1/2, y + 1/2$; (b) the 2D layer structure viewed along the *a* direction. The atoms of framework are shown in wires mode while those of coordinated DMSO and DMA molecules are shown in ball and stick mode; (c) the 2D layer structure viewed along the *b* direction; (d) the framework topology of the 2D net.

Cd–O_{DMA} bond distances are 2.488(2) Å and 2.352(2) Å, respectively, a little longer than that of Cd–O_{COOH} (2.270(2) Å and 2.463(2) Å). Additionally, the average Cd–N_{im} bond distance is 2.24(1) Å. To Cd(1), small deviations of bond angles from the idealized octahedral geometry are found for angles N(2A)–Cd(1)–N(1) [97.00(8)°], N(2A)–Cd(1)–O(2B) [145.14(8)°], N(1)–Cd(1)–O(2B) [117.47(8)°], N(2A)–Cd(1)–O(6) [88.98(8)°], N(1)–Cd(1)–O(6) [94.04(8)°], which implies that the metal ion has a distorted octahedral coordination polyhedron. Each ligand uses two imidazole nitrogen atoms to coordinate to two metal ions and the carboxylate group to chelate the third Cd²⁺ ion. Maybe due to the coordina-

tion to the metal ions, the ligand is distorted and a 79.76° dihedral angle is observed between the benzimidazole and benzene rings.

The combination of the 3-connected Cd(II) nodes and the ligands provides a 2D (4, 8) distorted network extending along the *bc* plane. As shown in Fig. 4b, the four-membered and eight-membered rings are almost parallel and perpendicular to the *a* direction respectively. The coordinated DMA molecules are captured in the eight-membered rings thus formed. Inside the layer, the Cd...Cd separations are 6.37 (bridged by the imidazole group) and 7.85 Å, respectively. A schematic representation of the 2D net is shown in Fig. 4c.

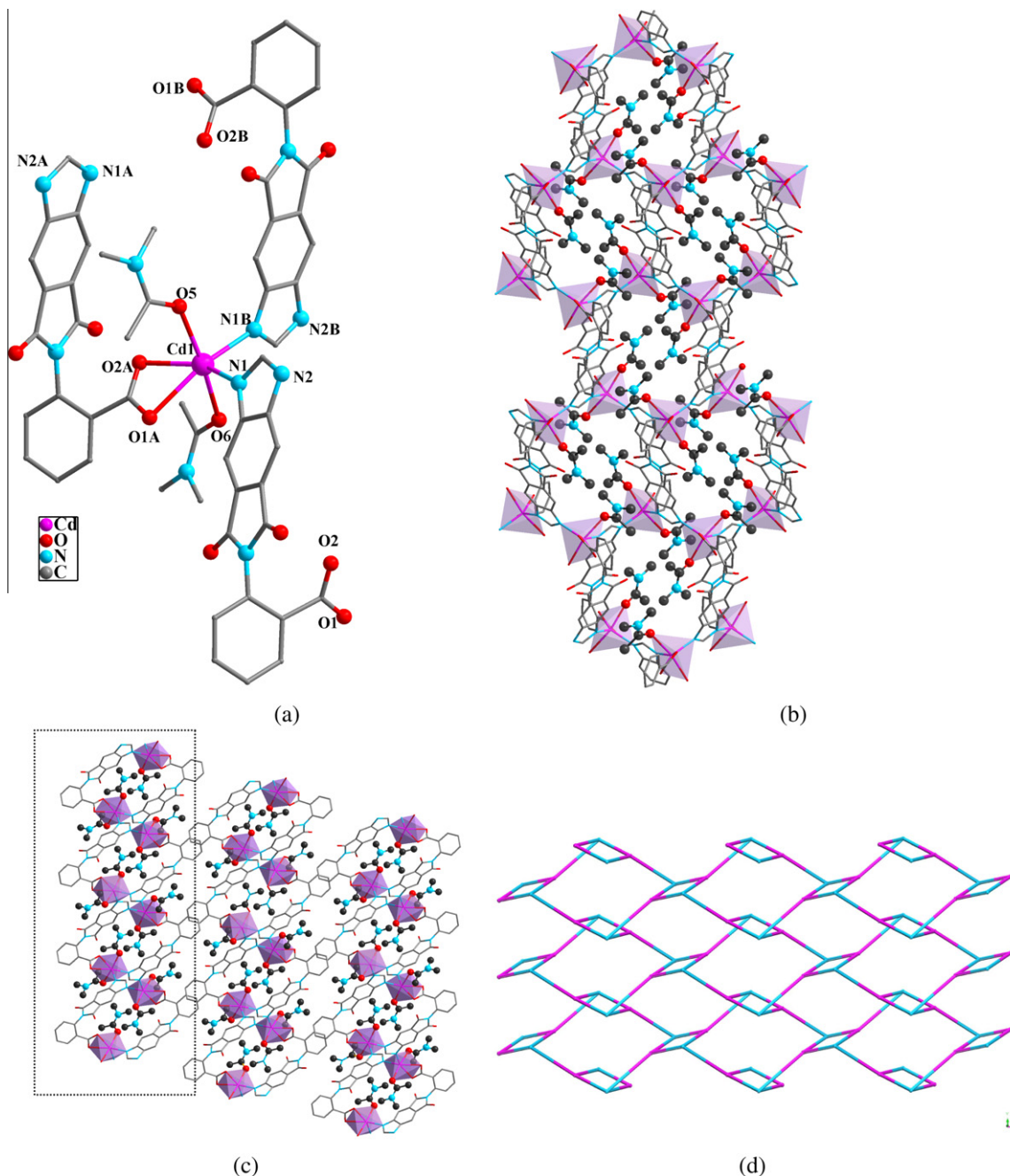


Fig. 4. The structure of compound **4**. (a) The coordination environment of the Cd^{2+} ion. Symmetry code: A: $-x + 1, y + 1/2, -z + 3/2$; B: $-x + 1, -y + 2, -z + 1$; (b) the 2D layer structure viewed along the a direction. The atoms of framework are shown in wires mode while those of coordinated DMA molecules are shown in ball and stick mode; (c) packing diagram of the 2D nets view along the b direction and (d) the framework topology of the 2D net.

3.5. The effect of torsion of the ligands on the structure of the compounds

Although the three ligands adopt $\mu_3\text{-}\eta_{\text{O}}^1: \eta_{\text{N}}^1: \eta_{\text{N}}^1; \mu_3\text{-}\eta_{\text{O}}^2: \eta_{\text{N}}^1: \eta_{\text{N}}^1; \mu_3\text{-}\eta_{\text{O}}^1: \eta_{\text{N}}^1: \eta_{\text{N}}^1$ and $\mu_3\text{-}\eta_{\text{O}}^2: \eta_{\text{N}}^1: \eta_{\text{N}}^1$ -coordination modes in the four compounds respectively, all of them can be treated as 3-connected nodes (Scheme 2). However, depending on the substituted sites of the carboxylate group on the benzene ring, the torsion angles of the three ligands are different and this does have an interesting effect on the final topology of the compounds. After coordination with the metal ion, the shape of 2-DPBB ligand can be described as trigonal pyramidal. This configuration makes it a good candidate for the construction of (4, 8) 2D net. However, in the case

of 4-DPBB ligand, the shape of the connector is more like a “Y” configuration. Strong hindrance effect prevents it from being used to build (4, 8) 2D net but (6, 3) 2D net. When the substituted carboxylate group is on the *meta*-position, the connector is in an intermediate state and can be used for the assembling of either (4, 8) or (6, 3) 2D net, by which the structures of **2** and **3** can be formed. These results clearly demonstrate that the torsion angle of the ligands plays an important role in the design of supramolecular structures.

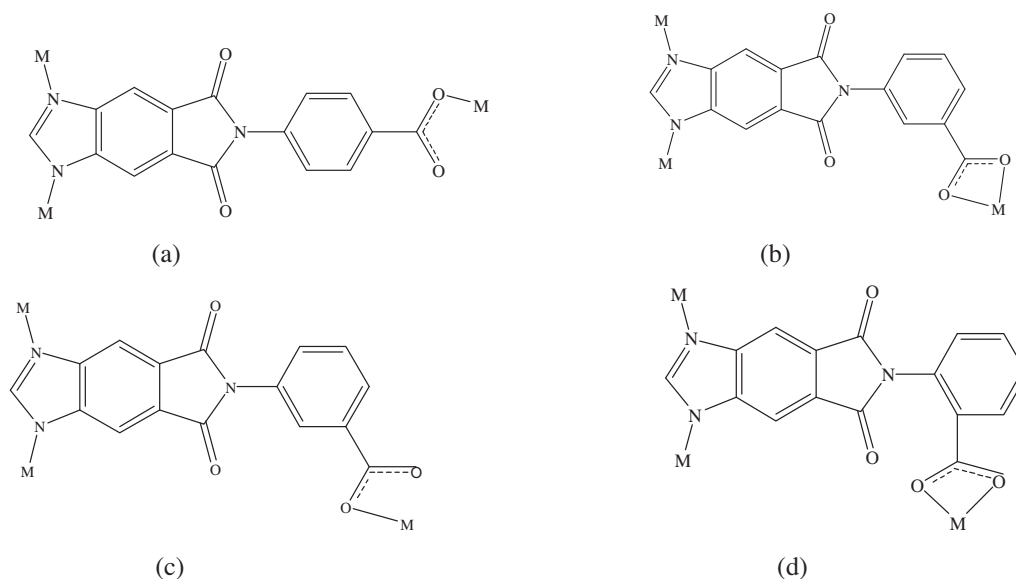
3.6. Syntheses and characterization of the compounds

Through the condensation reaction between benzimidazole-5,6-dicarboxylic acid and aminobenzoic acid in DMF solvent, three

Table 2
Bond lengths (Å) and angles (°) for the compounds.

1		2		3		4	
Zn(1)–O(1A)	1.962(6)	Cd(1)–N(2A)	2.215(3)	Cu(1)–O(3A)	1.945(2)	Cd(1)–N(2A)	2.235(2)
Zn(1)–O(5)	1.952(8)	Cd(1)–O(2B)	2.248(3)	Cu(1)–N(1)	1.991(2)	Cd(1)–N(1)	2.252(2)
Zn(1)–N(1)	1.971(6)	Cd(1)–N(1)	2.264(3)	Cu(1)–N(2B)	2.002(3)	Cd(1)–O(2B)	2.270(2)
Zn(1)–N(2B)	1.988(7)	Cd(1)–O(6)	2.382(3)	Cu(1)–O(5)	2.009(2)	Cd(1)–O(6)	2.352(2)
O(1)–Zn(1C)	1.962(6)	Cd(1)–O(5)	2.434(3)	Cu(1)–O(6)	2.486(2)	Cd(1)–O(1B)	2.463(2)
N(2)–Zn(1D)	1.988(7)	Cd(1)–O(1B)	2.486(3)			Cd(1)–O(5)	2.488(2)
O(5)–Zn(1)–O(1A)	107.1(3)	N(2A)–Cd(1)–O(2B)	146.9(1)	O(3A)–Cu(1)–N(1)	172.5(1)	N(2A)–Cd(1)–N(1)	97.00(8)
O(5)–Zn(1)–N(1)	108.3(3)	N(2A)–Cd(1)–N(1)	93.9(1)	O(3A)–Cu(1)–N(2B)	90.6(1)	N(2A)–Cd(1)–O(2B)	145.14(8)
O(1A)–Zn(1)–N(1)	124.3(3)	O(2B)–Cd(1)–N(1)	119.0(1)	N(1)–Cu(1)–N(2B)	95.8(1)	N(1)–Cd(1)–O(2B)	117.47(8)
O(5)–Zn(1)–N(2B)	106.7(3)	N(2A)–Cd(1)–O(6)	87.4(1)	O(3A)–Cu(1)–O(5)	87.46(9)	N(2A)–Cd(1)–O(6)	88.98(8)
O(1A)–Zn(1)–N(2B)	96.4(3)	O(2B)–Cd(1)–O(6)	91.8(1)	N(1)–Cu(1)–O(5)	86.2(1)	N(1)–Cd(1)–O(6)	94.04(8)
N(1)–Zn(1)–N(2B)	112.5(3)	N(1)–Cd(1)–O(6)	94.1(1)	N(2B)–Cu(1)–O(5)	177.95(9)	O(2B)–Cd(1)–O(6)	83.87(7)
C(16)–O(1)–Zn(1C)	108.0(5)	N(2A)–Cd(1)–O(5)	93.6(1)	C(16)–O(3)–Cu(1C)	108.1(2)	N(2A)–Cd(1)–O(1B)	94.88(8)
C(1)–N(1)–Zn(1)	121.7(5)	O(2B)–Cd(1)–O(5)	87.7(1)	S(1)–O(5)–Cu(1)	118.7(1)	N(1)–Cd(1)–O(1B)	156.94(8)
C(3)–N(1)–Zn(1)	133.5(5)	N(1)–Cd(1)–O(5)	85.0(1)	C(1)–N(1)–Cu(1)	122.9(2)	O(2B)–Cd(1)–O(1B)	55.09(7)
C(1)–N(2)–Zn(1D)	123.1(5)	O(6)–Cd(1)–O(5)	178.7(1)	C(2)–N(1)–Cu(1)	133.1(2)	O(6)–Cd(1)–O(1B)	105.88(7)
C(2)–N(2)–Zn(1D)	134.5(5)	N(2A)–Cd(1)–O(1B)	93.2(1)	C(1)–N(2)–Cu(1D)	130.6(2)	N(2A)–Cd(1)–O(5)	103.18(8)
C(8)–N(3)–C(9)	111.4(6)	O(2B)–Cd(1)–O(1B)	54.95(9)	C(3)–N(2)–Cu(1D)	125.7(2)	N(1)–Cd(1)–O(5)	84.58(8)
C(8)–N(3)–C(10)	127.0(6)	N(1)–Cd(1)–O(1B)	160.6(1)	C(9)–N(3)–C(8)	112.1(3)	O(2B)–Cd(1)–O(5)	86.05(7)
C(9)–N(3)–C(10)	121.6(6)	O(6)–Cd(1)–O(1B)	104.1(1)	(9)–N(3)–C(10)	122.7(3)	O(6)–Cd(1)–O(5)	167.83(7)
N(1)–C(1)–N(2)	116.5(7)	O(5)–Cd(1)–O(1B)	76.6(1)	C(8)–N(3)–C(10)	124.9(3)	O(1B)–Cd(1)–O(5)	73.49(8)

Symmetry transformations used to generate equivalent atoms. For **1**, A: $-x+3/2, y-1/2, -z+3/2$; B: $x+1, y, z$; C: $x-1, y, z$; D: $-x+3/2, y+1/2, -z+3/2$; For **2**, A: $-x+3/2, y-1/2, -z+3/2$; B: $x+1, y, z$; For **3**, A: $x-1/2, -y+3/2, z-1/2$; B: $-x+1/2, y+1/2, -z+1/2$; C: $x+1/2, -y+3/2, z+1/2$; D: $-x+1/2, y-1/2, -z+1/2$; For **4**, A: $-x+1, y+1/2, -z+3/2$; B: $-x+1, -y+2, -z+1$.



Scheme 2. Four coordination modes of the ligands.

new long rigid ligands bearing imidazolite/carboxylate groups, H₂4-DPBB, H₂3-DPBB, H₂2-DPBB, are obtained (Scheme 1). The formation of the coordination polymers is not significantly affected by the ratio of reactants. **1**, **2**, **3** and **4** are insoluble in water and common solvents.

The phase purity of **1–4** was confirmed by powder XRD analysis on bulk samples. The powder XRD profile of each as-synthesized compound is well matched with the simulated ones based on the single crystal X-ray structure (Fig. 5). To examine the thermal stabilities of the compounds, TGA experiments were performed by heating the crystalline sample from room temperature to 800 °C under nitrogen atmosphere (Fig. 6). In the TGA curve of **1** the first weight loss of 24.56% in the temperature region of 55–272 °C is due to the loss of free DMSO, MeOH and coordinated H₂O molecules (Calc. 23.23%). There is a long plateau in the temperature range of 272–547 °C, indicating a relatively high thermal stability

in the absence of solvent molecular. After 550 °C, the material shows a striking weight loss, indicating the completed decomposition of the structure. Curve **2** exhibits two distinct weight losses. The first step (28.0%) involves the loss of all the coordinated solvent molecules in the temperature region of 181–371 °C (Calc. 27.75%). In the second step, the material shows a striking weight loss, indicating the completed decomposition of the structure. In curve **3** the first weight loss of 29.6% in the temperature region of 80–300 °C corresponding to the loss of coordinated DMSO and DMA molecules (Calc. 30.9%). After 300 °C, the material exhibits a striking weight loss, indicating the completed decomposition of the structure. Curve **4** reveals two distinct weight losses. The first step (27.8%) involves loss of both coordinated DMA molecules in the temperature region of 78–291 °C (Calc. 29.40%). In the second step, the material shows a striking weight loss, indicating the completed decomposition of the structure. These results demonstrate

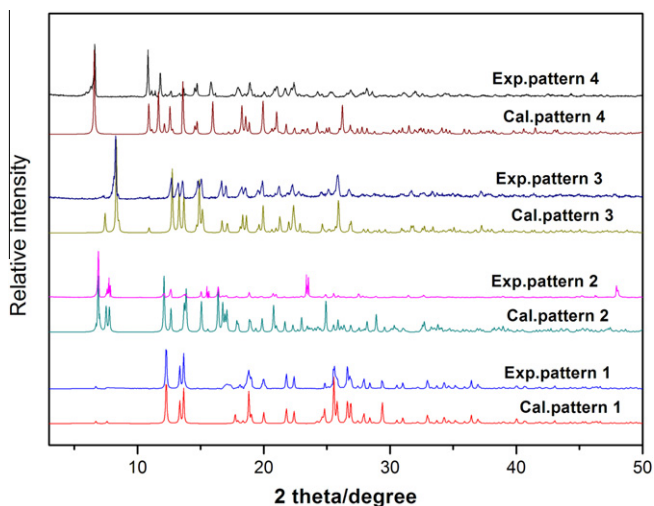


Fig. 5. Powder X-ray diffraction patterns of compounds 1–4.

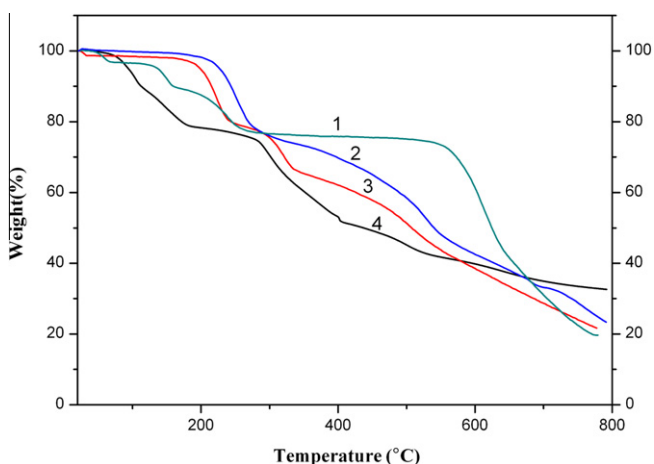


Fig. 6. Thermal stabilities of compounds 1–4.

that **1** is much more stable than the other three compounds. Such a high thermal stability is also well beyond those of most of the MOMs that are generally stable below 300 °C [28–31]. Considering the structures of the four compounds, the exceptional thermal stability of **1** can be attributed to the use of a more symmetrically rigid ligand. Several thermal stable MOMs based on symmetrically rigid ligands have been reported [28–31].

The luminescent properties of the ligands and **1–4** were checked in the solid state at ambient temperature (Fig. 7). The compounds and ligands show emission at 395–460 nm when excited at about 330 nm. For **1** and H₂4-DPBB ligand, intense fluorescent emissions at 454 nm and 460 nm were observed when excited at 320 nm. The 454 nm peak of **1** can be assigned as linker-localized $n \rightarrow p^*$ or $\pi \rightarrow \pi^*$ transition. **2** shows emission at 435 nm ($\lambda_{\text{ex}} = 300$ nm) which can also be attributed to the linker-localized transition as a 440 nm ($\lambda_{\text{ex}} = 300$ nm) emission was observed for H₂3-DPBB. **3** shows no emission which can be explained as the quenching effect due to the presence of transition-metal ion with unpaired electrons [34]. Compared with the 440 nm ($\lambda_{\text{ex}} = 332$ nm) emission peak of H₂2-DPBB, **4** has an apparent blue shift emission at 395 nm ($\lambda_{\text{ex}} = 332$ nm), which could be assigned to the emission of ligand-to-metal charge transfer (LMCT) [35,36]. The results indicate the substituted site of the carboxylate group on benzene ring do have some interesting effect on the fluorescent properties of the

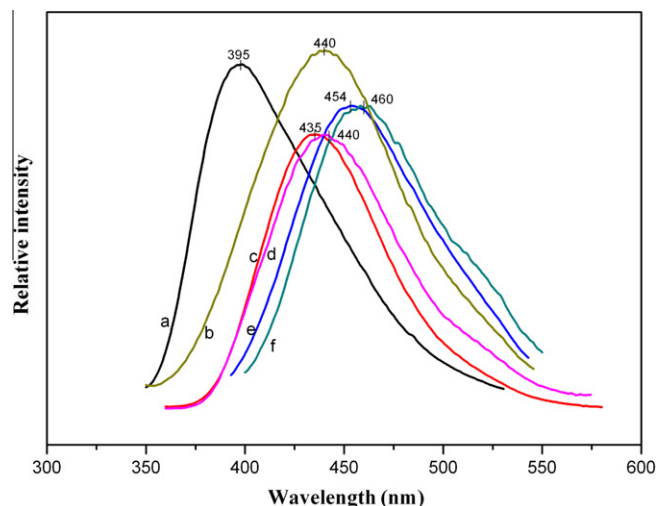


Fig. 7. The solid state fluorescence emission spectra for (a) **4** ($\lambda_{\text{ex}} = 332$ nm); (b) H₂2-DPBB ($\lambda_{\text{ex}} = 332$ nm); (c) **2** ($\lambda_{\text{ex}} = 300$ nm); (d) H₂3-DPBB ($\lambda_{\text{ex}} = 300$ nm); (e) **1** ($\lambda_{\text{ex}} = 320$ nm); (f) H₂4-DPBB ($\lambda_{\text{ex}} = 320$ nm).

compounds. When the substituted carboxylate group is on the *meta*- or *para*-position, only linker-localized emission is observed because of the mismatch of the energy level of the ligand with the energy levels of 3d¹⁰ metal ions. When the substituted carboxylate group is on the *ortho*-position, the two energy levels are matched and LMCT emission can be detected.

4. Conclusion

In summary, the syntheses, structures and properties of four 2D MOMs based on a series of new rigid imidazolate/carboxylate functionalized ligands are presented. The work shows that the substituted sites of the carboxylate group on the benzene ring of the ligands can influence the torsion degree of the three ligands, which can not only greatly affect the structures of the coordination polymers and resulted in two types of topology, but also the thermal stabilities and luminescent properties of the products. Thus the work represents a good example to reveal the relationship between ligands, structures and properties of the MOMs.

Acknowledgments

This material is based upon work supported by the National Science Foundation of China (21071025, 21101020 and 91122031), the Fundamental Research Funds for the Central Universities (DU-T12YQ04 and DUT11LK22), and fund of Ministry of Education of China (20100041120021 and ROCS).

Appendix A. Supplementary material

CCDC 870398–870401 contains the supplementary crystallographic data for this paper. These data can be obtained free of charge from The Cambridge Crystallographic Data Centre via www.ccdc.cam.ac.uk/data_request/cif. Supplementary data associated with this article can be found, in the online version, at <http://dx.doi.org/10.1016/j.ica.2012.07.031>.

References

- [1] J.W. Steed, J.L. Atwood, *Supramolecular Chemistry*, Wiley and Sons, New York, 2000.
- [2] G. Férey, *Chem. Soc. Rev.* 37 (2008) 191.
- [3] J.A.A.W. Elemans, S. Lei, S.D. Feyter, *Angew. Chem., Int. Ed.* 40 (2009) 7298.

- [4] R. Ali, H. Shima, M. Ali, *Coord. Chem. Rev.* 253 (13–14) (2009) 1882.
- [5] B. Moulton, M.J. Zaworotko, *Chem. Rev.* 101 (2001) 1629.
- [6] A. Phan, C.J. Doonan, F.J. Uribe-Romo, C.B. Knobler, O.M. Yaghi, *Acc. Chem. Res.* 43 (2010) 58.
- [7] J.R. Li, R.J. Kuppler, H.C. Zhou, *Chem. Soc. Rev.* 5 (2009) 1477.
- [8] L. Pan, E.B. Woodlock, X.T. Wang, C. Zheng, *Inorg. Chem.* 39 (2000) 4174.
- [9] S.Y. Yang, L.S. Long, Y.B. Jiang, R.B. Huang, L.S. Zheng, *Chem. Mater.* 14 (2002) 3229.
- [10] D.J. Tranchemontagne, J.L. Mendoza-Cortes, M. O'Keeffe, *Chem. Soc. Rev.* 5 (2009) 1257.
- [11] A. Tabacaru, C. Pettinari, N. Masciocchi, S. Galli, F. Marchetti, M. Angjellari, *Inorg. Chem.* 50 (2011) 11506.
- [12] V. Colombo, S. Galli, H.J. Choi, G.D. Han, A. Maspero, G. Palmisano, N. Masciocchi, J.R. Long, *Chem. Sci.* 2 (2011) 1311.
- [13] C. Di Nicola, F. Garau, M. Gazzano, M. Monari, L. Pandolfo, C. Pettinari, R. Pettinari, *Cryst. Growth Des.* 10 (2010) 3120.
- [14] E.Q. Procopio, F. Linares, C. Montoro, V. Colombo, A. Maspero, E. Barea, J.A.R. Navarro, *Angew. Chem., Int. Ed.* 49 (2010) 7308.
- [15] J.J. Perry IV, J.A. Perman, M.J. Zaworotko, *Chem. Soc. Rev.* 38 (2009) 1400.
- [16] L. Hamon, C. Serre, T. Devic, *J. Am. Chem. Soc.* 131 (25) (2009) 8775.
- [17] B. Wang, A.P. Côté, H. Furukawa, M. O'Keeffe, O.M. Yaghi, *Nature* 453 (2008) 207.
- [18] Z.Q. Wang, S.M. Cohen, *Chem. Soc. Rev.* 38 (2009) 1315.
- [19] A. Phan, C.J. Doonan, F.J. Uribe-Romo, C.B. Knobler, M. O'Keeffe, O.M. Yaghi, *Acc. Chem. Res.* 43 (1) (2010) 58.
- [20] R. Banerjee, A. Phan, B. Wang, C. Knobler, H. Furukawa, M. O'Keeffe, O.M. Yaghi, *Science* 319 (5865) (2008) 939.
- [21] R. Banerjee, H. Furukawa, D. Britt, C. Knobler, M. O'Keeffe, O.M. Yaghi, *J. Am. Chem. Soc.* 131 (11) (2009) 3875.
- [22] H. Wu, W. Zhou, T. Yildirim, *J. Am. Chem. Soc.* 129 (17) (2007) 5314.
- [23] M.H. Alkordi, J.A. Brant, L. Wojtas, V.C. Kravtsov, A.J. Cairns, M. Eddaoudi, *J. Am. Chem. Soc.* 131 (2009) 17753.
- [24] X.M. Jing, H. Meng, G.H. Li, Y. Yu, Q.S. Huo, M. Eddaoudi, Y.L. Liu, *Cryst. Growth Des.* 10 (2010) 3490.
- [25] R.Q. Fang, X.M. Zhang, *Inorg. Chem.* 45 (2006) 4801.
- [26] W.G. Lu, C.Y. Su, T.B. Lu, L. Jiang, J.M. Chen, *J. Am. Chem. Soc.* 128 (2006) 34.
- [27] Z.G. Guo, R. Cao, X.J. Li, D.Q. Yuan, W.H. Bi, X.D. Zhu, Y.F. Li, *Eur. J. Inorg. Chem.* 5 (2007) 742.
- [28] S.Y. Yang, L.S. Long, Y.B. Jiang, L.S. Zheng, *Chem. Mater.* 14 (2002) 3229.
- [29] N. Masciocchi, G.A. Ardizzoia, G. LaMonica, A. Maspero, A. Sironi, *Eur. J. Inorg. Chem.* (2000) 2507.
- [30] C.H. Jiang, L.F. Song, C.L. Jiao, J. Zhang, L.X. Sun, F. Xu, Y. Du, Z. Cao, *J. Therm. Anal. Calorim.* 103 (2011) 373.
- [31] J. Zhang, J.L. Zeng, Y.Y. Liu, L.X. Sun, F. Xu, W.S. You, Y. Sawada, *J. Therm. Anal. Calorim.* 91 (2008) 189.
- [32] SMART, SAINT and SADABS. Bruker AXS Inc.: Madison, WI; 1998.
- [33] G.M. Sheldrick, *S^{helx}-97*, Program for X-ray Crystal Structure Refinement, University of Göttingen, Germany, 1997.
- [34] M.D. Allendorf, R.K. Bhakta, R.J.T. Houka, *Chem. Soc. Rev.* 38 (2009) 1330.
- [35] X.D. Guo, G.S. Zhu, Q.R. Fang, M. Xue, G. Tian, J.Y. Sun, X.T. Li, S.L. Qiu, *Inorg. Chem.* 44 (2005) 3850.
- [36] J.C. Dai, X.T. Wu, Z.Y. Fu, C.P. Cui, S.M. Hu, W.X. Du, L.M. Wu, H.H. Zhang, R.Q. Sun, *Inorg. Chem.* 41 (2002) 1391.